Stationary localized solutions in binary convection in slightly inclined rectangular cells

Arantxa Alonso,* Oriol Batiste,† and Isabel Mercader‡
Departament de Física, Universitat Politècnica de Catalunya, Mòdul B4, 08034 Barcelona, Spain

(Received 13 July 2022; accepted 25 October 2022; published 16 November 2022)

We analyze numerically the effect of a slight inclination in the lowest part of the snaking branches of convectons that are present in negative separation ratio binary mixtures in two-dimensional elongated rectangular cells. The exploration reveals the existence of novel stationary localized solutions with striking spatial features different from those of convectons. The numerical continuation of these solutions with respect to the inclination of the cell unveils the existence of even further families of localized structures that can organize in closed branches. A variety of localized solutions coexist for the same heating and inclination, depicting a highly complex scenario for solutions in the lowest part of the snaking diagrams for moderate to high heating. The different localized solutions obtained in the horizontal cell are discussed in detail.

DOI: 10.1103/PhysRevE.106.055106

I. INTRODUCTION

Thermal convection is an important problem with relevant implications to many geophysical flows and a multitude of technological applications. The flow patterns that are observed for simple incompressible fluid convection are highly enriched by the consideration of binary fluid mixtures. Binary fluid convection has indeed been used for many years as a prototypical system for the study of the transition to chaos in a fluid flow. In binary mixtures thermal convection promoted by thermal gradients may be enhanced by concentration nonuniformities sustained by the Soret effect, i.e., the generation of concentration fluxes by temperature gradients. The components of miscible ordinary two-component mixtures tend to separate in an imposed thermal gradient, and this separation, in turn, alters the driving force for convection. The Soret effect is quantified by the Soret coefficient (separation ratio, in nondimensional form).

A relevant configuration for the study of pattern formation, and the reference setup for our work, is that of a horizontal closed rectangular box heated from below. When mixtures with a negative Soret coefficient are used, i.e., mixtures in which the heavier component of the fluid is driven into the direction of higher temperature, the conduction state loses stability via a Hopf bifurcation that can lead to a rich dynamical behavior near threshold. Experiments performed in the late 1980s [1–4] and subsequent detailed numerical studies [5–9] showed that a variety of interesting spatially extended and localized patterns arise in this configuration.

Among these localized structures, the so-called *convectons* raised a lot of interest in the dynamical-systems community in the recent past. Binary fluid convection is perhaps the first fluid system where these states were observed experimentally, using horizontal annular containers heated from below [10]. Convectons in binary mixtures consist of regions of large-amplitude stationary convection coexisting with regions of quiescent fluid and were obtained numerically a few years later [11]. In subsequent works in two-dimensional horizontally extended domains convectons were shown to be located in snakes-and-ladders branches of solutions, which allow a large multiplicity of coexisting convectons of different lengths and types [7–9,12]. Convectons arranged in analogous snaking branches of solutions were also computed in natural doubly diffusive convection in a two-dimensional vertically extended cavity, with thermal and concentration horizontal gradients allowing the existence of a conduction state [13,14]. This phenomenology is essentially captured by the bistable Swift-Hohenberg equation [12,15]. Significantly, three-dimensional doubly diffusive convectons that now arrange in primary and secondary snaking branches were obtained numerically in a closed vertically extended domain [16].

Although most of the properties of convectons in two-dimensional (2D) rectangular cells heated from below are now well established, some features remain unexplored. In particular, it is well known that when the system possesses reflection symmetry in the midplane (i.e., Boussinesq symmetry) the two snaking branches correspond to two types of stationary convectons: even and odd convectons. The intertwined branches of localized states with different symmetry are interconnected by rung-like branches consisting of asymmetric localized states. As one proceeds up the snaking branches the localized states grow in length by nucleating new rolls on either side in such a way that the symmetry of the state is preserved. When the domain is almost filled, the snaking must cease and the two snaking branches turn continuously into large-amplitude domain-filling states. However, the study of the lowest part of the snaking branches when the heating (parametrized by the Rayleigh number) is increased has never been addressed in binary mixtures and will be the focus of the present study.

*arantxa.alonso@upc.edu
†oriol.batiste@upc.edu
‡maria.isabel.mercader@upc.edu

The recent numerical study of Mercader *et al.* [17] explores the effect of slightly tilting rectangular elongated cells for negative Soret mixtures and shows that bifurcation diagrams are significantly altered. With the small breaking of symmetry induced by inclination, it might be expected beforehand that (i) the solution branch corresponding to the large-scale base flow that replaces the conduction state in the inclined system extends to large values of the Rayleigh number without significant change and (ii) the inclination splits the snaking branch of odd convectons into two branches of states that inherit the symmetry of the odd convectons, while the snaking branch of even convectons breaks up into disconnected branches of asymmetric states. These changes in the bifurcation diagram are only observed for very small inclinations and both the behavior of the large-scale base flow branch, and the organization of the large-amplitude localized solutions in snaking branches, undergo a profound change as the inclination increases. The snaking bifurcation diagram present in the noninclined system is destroyed already at small inclinations and for slightly larger but still small inclinations new localized states lying on solution branches with very complex behavior are obtained. Other examples in which the snaking diagrams do not persist are discussed in the recent works of Lo Jacono *et al.* [18] in doubly diffusive convection in a vertical slot when changing the boundary condition at one of the vertical walls and of Azimi and Schneider [19] in plane Couette flow with wall-normal suction. The effect of adding a slight inclination in extended layers of binary mixtures heated from below was also studied in a shallow cylinder filled with a positive Soret mixture [20,21]. The results on both tilted problems suggest that even very small inclinations produce substantial changes in the flow structure and result in new phenomena.

Motivated by the evidence that very slight inclinations affect substantially the dynamics, we aim to explore the lowest part of the snaking branches for different inclinations of the cell when the heating is increased. We will use numerical continuation techniques and perform parametric continuation in the Rayleigh number and inclination to elucidate the type of solutions that arise in this region of the diagrams. The study unveils the existence of localized solutions that are also present in the noninclined cell and that exhibit striking spatial features different from those of convectons. As we will see, the depicted scenario in the lowest part of the snaking diagrams for moderate to high heating is very complex.

The organization of the paper is as follows. In Sec. II, we formulate the equations and boundary conditions, summarize the symmetries of the system, and explain the numerical methods used. The main results are presented and discussed in Sec. III. In particular, Sec. III A describes the solutions that appear in the lowest part of the snaking branches when the heating is increased for the horizontal $\alpha = 0$ cell and for the $\alpha = 0.01$ and $\alpha = 0.03$ inclined cells, and Sec. III B summarizes the results obtained by numerical continuation with respect to the inclination of the cell of some of the striking small amplitude localized states previously identified. Finally, a summary of the main results of the work is discussed in Sec. IV.

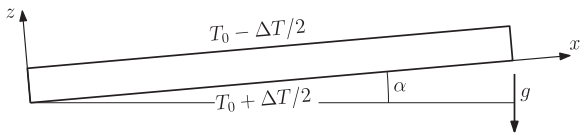

FIG. 1. Sketch of the domain geometry.

II. FORMULATION OF THE PROBLEM: EQUATIONS, SYMMETRIES, AND NUMERICAL METHODS

We consider two-dimensional Boussinesq binary fluid convection in a rectangular cell of height H and length L, inclined at a small angle α with respect to the horizontal. The cell is heated from below, with ΔT being the temperature difference between the bottom and the top. We choose coordinates whose origin is located at the bottom left corner and oriented along the bottom wall (the x direction) and the side wall (the z direction). In terms of these coordinates the acceleration due to gravity takes the form

$$\mathbf{g} = -g\sin\alpha\,\hat{\mathbf{e}}_x - g\cos\alpha\,\hat{\mathbf{e}}_z.$$

A sketch of the domain geometry is shown in Fig. 1.

We split the temperature T and concentration of the heavier molecular weight component C_{heavy} into a linear profile in z and fluctuations Θ^* and Σ^* as follows:

$$\begin{aligned} T &= T_0 + \Delta T(1/2 - z/H) + \Theta^*, \\ C_{\text{heavy}} &= C_0 - C_0(1-C_0)S_T\Delta T(1/2 - z/H) + \Sigma^*, \end{aligned} \quad (1)$$

where T_0 and C_0 are the values of the temperature and concentration at midheight and S_T is the Soret coefficient, hereafter assumed to be negative so that the heavier component migrates towards the lower boundary in response to the applied temperature difference. Here H is the height of the cell. With this decomposition the mass flux only depends on the gradient of Θ^* and Σ^*, the superscript * indicates the unscaled quantities.

Scaling lengths with H, time with the vertical thermal diffusion time H^2/κ, κ being the thermal diffusivity, temperature with ΔT, and concentration with the induced concentration difference $-C_0(1-C_0)S_T\Delta T$, we obtain the following dimensionless equations describing inclined binary fluid convection:

$$\begin{aligned} \mathbf{u}_t + (\mathbf{u}\cdot\nabla)\mathbf{u} &= -\nabla P + \sigma\nabla^2\mathbf{u} + \mathrm{Ra}_z\sigma[(1+S)\Theta + S\eta]\hat{\mathbf{e}}_z \\ &\quad + \mathrm{Ra}_x\sigma[(1+S)\Theta + S\eta]\hat{\mathbf{e}}_x \\ &\quad - \mathrm{Ra}_x\sigma(1+S)(z-1/2)\hat{\mathbf{e}}_x, \\ \Theta_t + (\mathbf{u}\cdot\nabla)\Theta &= w + \nabla^2\Theta, \\ \eta_t + (\mathbf{u}\cdot\nabla)\eta &= -\nabla^2\Theta + \tau\nabla^2\eta, \end{aligned} \quad (2)$$

together with the incompressibility condition

$$\nabla\cdot\mathbf{u} = 0. \quad (3)$$

Here $\mathbf{u} \equiv (u, w)$ denotes the nondimensional velocity field, P is the nondimensional mechanical pressure that includes parts of the buoyancy term that can be written as a gradient, Θ is the nondimensional temperature fluctuation, and $\eta \equiv \Sigma - \Theta$, where Σ represents the nondimensional concentration

fluctuation. The variable η is defined such that its gradient is proportional to the dimensionless mass flux.

The system is thus specified by the inclination angle α and four dimensionless parameters: the Rayleigh number Ra that provides a dimensionless measure of the imposed temperature difference ΔT, the separation ratio S proportional to the Soret coefficient S_T that measures the concentration contribution to the buoyancy force due to cross-diffusion, and the Prandtl and Lewis numbers σ, τ, in addition to the aspect ratio Γ of the rectangular cell. These parameters are defined as follows:

$$\mathrm{Ra} = \frac{\gamma g \Delta T H^3}{\kappa \nu}, \quad S = C_0(1-C_0)\frac{\beta}{\gamma}S_T, \quad \sigma = \frac{\nu}{\kappa},$$
$$\tau = \frac{D}{\kappa}, \quad \Gamma = \frac{L}{H},$$

where γ and β are the thermal and concentration expansion coefficients, D is the solute diffusivity, and ν is the kinematic viscosity. In these equations $\mathrm{Ra}_x = \mathrm{Ra}\sin\alpha$ and $\mathrm{Ra}_z = \mathrm{Ra}\cos\alpha$.

We consider here the boundary conditions corresponding to impermeable, no-slip boundaries with fixed imposed temperature at the top and bottom and thermally insulating sidewalls. Thus

$$u = w = \Theta = \eta_z = 0 \quad \text{on} \quad z = 0, 1, \tag{4}$$

and

$$u = w = \Theta_x = \eta_x = 0 \quad \text{on} \quad x = 0, \Gamma. \tag{5}$$

We evaluate, as an estimate of the strength of the convection, the dimensionless velocity norm E defined by

$$E = \Gamma^{-1}\int_{z=0}^{z=1}\int_{x=0}^{x=\Gamma} \mathbf{u}\cdot\mathbf{u}\, dx\, dz.$$

This quantity represents twice the kinetic energy per unit area of the system. In the following we refer to E as the mean kinetic energy.

When $\alpha \neq 0$ the equations, together with the boundary conditions, are equivariant with respect to the symmetry group $Z_2 = \{I, R\}$, where I stands for the identity and R is a reflection with respect to the center of the cell. Specifically, the reflection R acts on the fields u, w, the stream function Ψ ($u = -\Psi_z$, $w = \Psi_x$), Θ, and η as follows:

$$R : (x, z) \to (\Gamma - x, 1 - z),$$
$$(u, w, \Psi, \Theta, \eta) \to (-u, -w, \Psi, -\Theta, -\eta). \tag{6}$$

As a consequence, the equations admit solutions invariant under R as well as solutions that break the symmetry R. In the later case the application of R to a nonsymmetric solution generates a distinct but symmetry-related solution. When $\alpha = 0$, i.e., the layer is horizontal, the symmetry group is enlarged and becomes the symmetry group D_2 generated by two separate reflections R_1 and R_2, where R_1 corresponds to a reflection in the vertical $x = \Gamma/2$ plane and R_2 to a reflection in the horizontal $z = 1/2$ plane:.

$$R_1 : (x, z) \to (\Gamma - x, z),$$
$$(u, w, \Psi, \Theta, \eta) \to (-u, w, -\Psi, \Theta, \eta), \tag{7}$$

$$R_2 : (x, z) \to (x, 1 - z),$$
$$(u, w, \Psi, \Theta, \eta) \to (u, -w, \Psi, -\Theta, -\eta). \tag{8}$$

Notice that the reflection R can be obtained as $R = R_1 \circ R_2$.

For $\alpha \neq 0$, the system is no longer equivariant with respect to the symmetry R_1, but a solution of the system with inclination α, transformed by R_1, is a solution of the system with inclination $-\alpha$. We say that the system possesses the following symmetry $R_{1,\alpha}$, related to the reversed inclination

$$R_{1,\alpha} : (\alpha, x, z) \to (-\alpha, \Gamma - x, z),$$
$$(u, w, \Psi, \Theta, \eta) \to (-u, w, -\Psi, \Theta, \eta). \tag{9}$$

The system of Eqs. (2) and (3) and boundary conditions (4) and (5) was solved numerically using the algorithm described in [22], which can be summarized as follows. To integrate the equations in time, we use the second-order time-splitting method proposed by the authors of [23] combined with a pseudospectral method for the spatial discretization, Chebyshev collocation in x and z. The Helmholtz equations obtained as a result of the splitting are solved using a diagonalization technique [24].

Steady solutions were computed with Newton's method. We used a first-order version of the time-stepping code described above for the calculation of a Stokes preconditioner that allows a matrix-free inversion of the preconditioned Jacobian needed in each Newton iteration [25]. The corresponding linear system is solved by an iterative technique using the GMRES package [26]. The left-hand side of the preconditioned linear system (Jacobian acting on the correction) corresponds to one time step of the linearized equations and the right-hand side corresponds to performing one time step of the full nonlinear equations. In this way the Jacobian matrix is never constructed or stored [25]. The convergence criterion for the Newton method is 10^{-7}.

In the results reported in the present paper we used a resolution that ensures variations of the mean kinetic energy E smaller than 0.1%. We used a grid of $n_x = 640$ and $n_z = 32$ points in the x and z directions, respectively.

III. RESULTS

We consider a negative separation ratio binary mixture of nondimensional parameters $S = -0.1$, $\tau = 0.01$, and $\sigma = 7$, representative of water-ethanol mixtures and previously used in earlier works [7–9]. The mixture fills a two-dimensional rectangular $\Gamma = 14$ cell. Results for the horizontal $\alpha = 0$ case and for very small values of inclination are presented.

Previous studies of this system, for the set of parameter values of interest in this work, show that the primary bifurcation of the $\alpha = 0$ conduction state is a subcritical Hopf bifurcation that takes place at $\mathrm{Ra}_{\mathrm{Hopf}} = 1947.5$ [6]. With further increase in the Rayleigh number, the system evolves either to finite-amplitude oscillatory states (chevrons, blinking states, and repeated transients [5]) or towards steady convection. The steady convection can either fill the domain or form localized time-independent *convectons*. The binary mixture convectons are organized within a snaking region $\mathrm{Ra}_- < \mathrm{Ra} < \mathrm{Ra}_+$ in the Rayleigh number Ra. Within this region one finds *even convectons*, which are invariant under R_1,

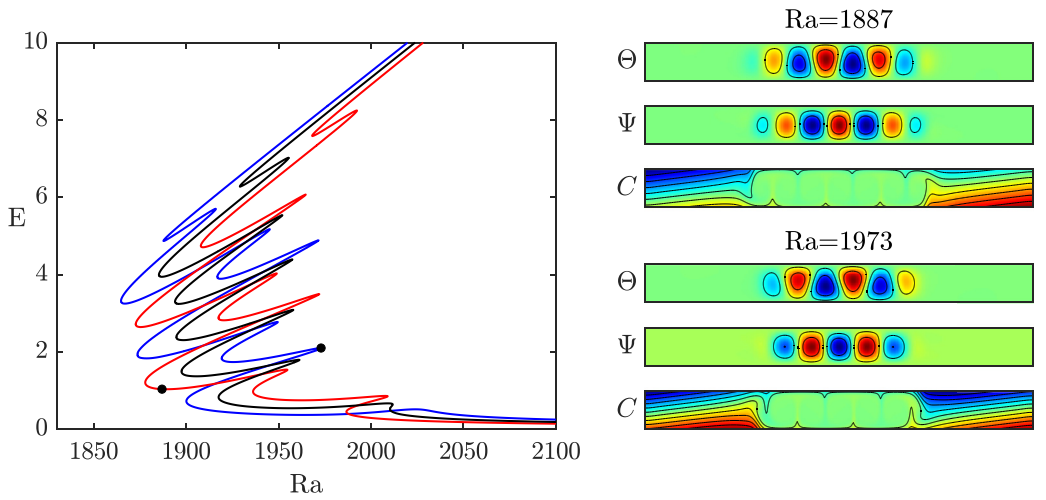

FIG. 2. Snaking branches showing the splitting of the odd convecton branch for $\alpha = 0$ (black curve) when $\alpha = 0.01$ (blue and red curves). The states on the blue or red curves correspond to states with a counterclockwise or clockwise central roll (CCW or CW branches, respectively). The panels on the right show contour plots of temperature fluctuation Θ, streamfunction Ψ, and concentration C for the two clockwise or counterclockwise central roll states indicated by the solid dots on the solution branch (Ra = 1887 and Ra = 1973). Parameters: $S = -0.1$, $\tau = 0.01$, $\sigma = 7$, and $\Gamma = 14$.

and *odd convectons*, which are invariant under $R = R_1 \circ R_2$. Convectons lie on distinct solution branches that snake back and forth across the snaking region. The snaking interval contains a large multiplicity of coexisting odd and even convectons of different lengths, many of which turn out to be numerically stable [11,27]. In a bifurcation diagram showing a global quantity, such as the kinetic energy, as a function of the Rayleigh number, each point in the snaking branches corresponds to two different solutions. These two solutions with the same value of the global quantity are related by the R_1 symmetry if they lie on the odd convecton branch of R-invariant states and are related by the R symmetry if they lie on the even convecton branch of R_1-invariant states [9].

When the cell is slightly inclined the character of the problem changes dramatically because of the generation of a large-scale flow (LSF) along the bottom and top walls. The LSF is now the unique solution at very low Ra and its net effect is to generate isocontours of concentration with constant slope, except very close to the sidewalls where the slope must vanish. For very small inclinations, the LSF flow destabilizes in a primary Hopf bifurcation that either respects or breaks its R symmetry, giving rise to several time-dependent patterns resembling those of the noninclined cell case. For larger but still small inclinations, at $\alpha = 0.047$, this bifurcation no longer exists and the base flow undergoes a fold bifurcation at a low value of Ra [17].

When $\alpha \neq 0$ the equations continue to admit R-invariant solutions. We call these solutions *odd states*, in analogy with the name used in the $\alpha = 0$ case. Figure 2(a) shows the snaking diagram (kinetic energy E as a function of the Rayleigh number Ra) for the R-invariant states obtained for $\alpha = 0.01$. Since the symmetry R_1 is broken, the odd branch of the $\alpha = 0$ cell necessarily splits into two for $\alpha \neq 0$, leading to the blue and red R-symmetric snaking branches shown in Fig. 2(a). This plot also includes the snaking diagram for the odd states when $\alpha = 0$ (black curve). Figure 2(b) shows the concentration C, the stream function Ψ, and temperature Θ contour plots for states on the blue and red branches. Notice that, to improve the visualization of the flow pattern, the aspect ratio of the cell is not preserved in the contour-plot diagrams. Unlike in Fig. 1, from now on, the aspect ratio in the diagrams is smaller than 14, and this fact distorts slightly the perception of the actual roll aspect ratio. States on the blue branch are characterized by a *counterclockwise central roll* in the convective region (solution obtained for Ra = 1973, with a blue central roll in the Ψ contour plot), while states on the red branch have a *clockwise central roll* (solution obtained for Ra = 1887, with a red central roll in the Ψ contour plot). Because of the pumping action associated with odd states [7,11], the previous state entrains heavier fluid from below on the right and lighter fluid from top on the left. The result is a marked positive gradient in the contours of constant concentration C. Similar pumping takes place in the later case, but because of the reversed circulation of the outer rolls the entrainment direction is reversed, resulting in a much starker left-right asymmetry in the concentration profile. Hereinafter we call the blue and red branches the counterclockwise central roll (CCW) and clockwise central roll (CW) branches.

The results we present in this work focus on the behavior of the lowest part of the snaking branches when the Rayleigh number Ra is increased for the R-invariant solutions (odd solutions). We aim at clarifying the role of small inclinations of the cell on the small amplitude solutions arising in this part of the snaking diagrams. To do this, as a first step, we will perform parametric continuation in Rayleigh number Ra of solutions in the lowest part of the snaking and, as a second step, we will do a continuation in the inclination α of selected localized solutions with outstanding features obtained previously. The results obtained when Ra is varied are presented in Sec. III A and those obtained when α is varied are discussed in Sec. III B. The disconnected branches of asymmetric states that arise after the snaking branch of even convectons breaks

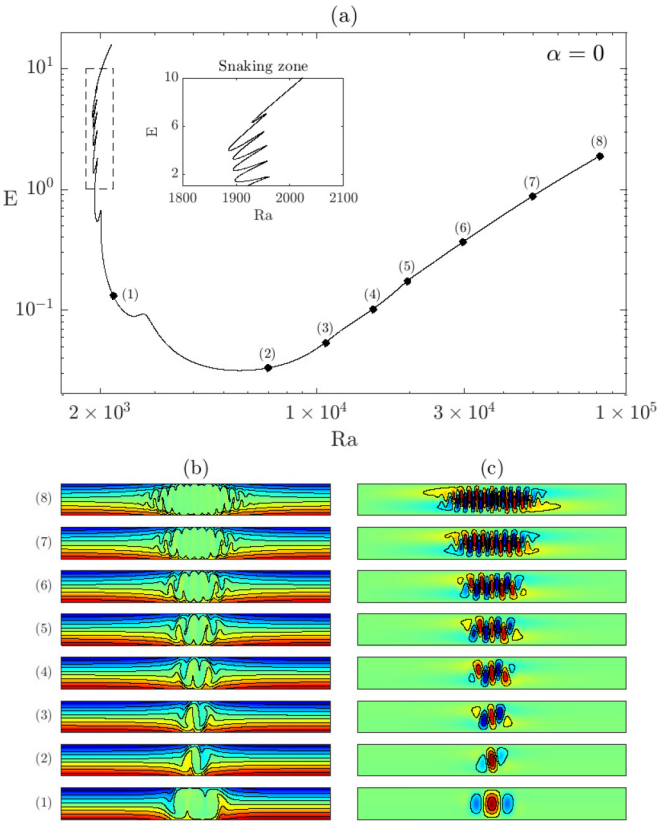

FIG. 3. (a) Solution branch obtained by numerical continuation of the lowest part of the snaking branch of odd states when the Rayleigh number Ra is increased, for $\alpha = 0$. The inset shows an enlargement of part of the snaking zone. Contour plots of (b) concentration C and (c) stream function Ψ at the locations indicated in panel (a). In the concentration contour plots the same color bar is used for all states. Parameters: $S = -0.1$, $\tau = 0.01$, $\sigma = 7$, and $\Gamma = 14$.

up when inclination is introduced are not considered in this paper.

A. Numerical continuation of small-amplitude localized solutions with respect to Ra

To begin the study of the lowest part of the snaking diagrams as the Rayleigh number Ra increases we consider first the horizontal $\alpha = 0$ cell and focus on the odd snaking branch of solutions, which is the branch that persists when inclination is introduced. Then we discuss the results for inclinations $\alpha = 0.01$ and $\alpha = 0.03$. With inclination, each value of α includes the analysis of the two odd snaking branches resulting from the splitting of the single $\alpha = 0$ odd branch.

1. Horizontal $\alpha = 0$ cell: Small-wavelength localized states

For $\alpha = 0$, the numerical continuation of the odd snaking branch for large values of Ra reveals that the lowest part of the convecton snaking branch does not connect to the base conductive state. Figure 3 shows the lowest part of the branch of odd convectons when continued up to Ra $\approx 10^5$. Figure 3(a) shows the kinetic energy E as a function of Ra, and Figs. 3(b) and 3(c) the contour plots of concentration C and stream function Ψ at the locations indicated in Fig. 3(a). We appreciate a marked increase of the kinetic energy of the solutions in the low part of the diagram for the largest values of Ra, associated to a slow growth of the size of the convective region in the localized structure (the number of convection rolls increases). Still more remarkable the wavelength of the rolls decreases considerably, giving rise to a peculiar localized pattern in which the convective rolls appear tightly packed one against each other.

The behavior we observe for mixtures of sufficiently negative values of the separation ratio and parameter values similar to those used in this paper is not specific of the two-dimensional closed container. We computed the lowest part of the snaking branch in the case of periodic boundary conditions in the lateral walls of the container and the same behavior is obtained.

2. Tilted $\alpha = 0.01$ cell: Highly localized states and two-pulse snaking

For $\alpha = 0.01$, the numerical continuation with Ra of the lowest part of the two odd snaking branches coming from the splitting of the $\alpha = 0$ case [CW and CCW branches in Fig. 2(b)] shows that the branches do not necessarily increase monotonically to large values of the Rayleigh number. In one of the branches, the convective region of the pattern remains rather small while the amplitude of the solution slowly grows; in the other, the branch turns around in a fold and eventually reenters the snaking region. We analyze the two cases in more detail.

Figure 4 shows the results obtained when the lowest part of the CCW odd branch of convectons (counterclockwise central roll in the snaking region) is continued to large values of Ra (up to Ra $\approx 10^5$) for an inclination of $\alpha = 0.01$. Figure 4(a) shows the kinetic energy as a function of Ra, and Figs. 4(b) and 4(c) the contour plots of concentration C and stream function Ψ at the locations indicated in Fig. 4(a). As can be appreciated in the concentration contour plots, a background concentration slope appears as a result of the large-scale flow induced by inclination. The initial part of the curve and the structure of patterns (1), (2), and (3) are quite similar to that observed in the $\alpha = 0$ case (the kinetic energy increases initially with Ra). But sudden back and forth oscillations producing two clearly visible peaks in the curve of kinetic energy take place between Ra $\sim 2.793 \times 10^4$ and Ra $\sim 2.248 \times 10^4$, and between Ra $\sim 3.857 \times 10^4$ and Ra $\sim 2.873 \times 10^4$. In the first peak, the notable increase of the kinetic energy (4) is followed by an abrupt decrease (5). Within this region, the central roll of the solutions splits and a new solution with two pairs of vertical stacked rolls is obtained. In the second peak, a new increase and decrease of the kinetic energy takes place again. The solutions within this region of the curve show a separation of the stacked pairs of rolls (6), a generation of a counterclockwise central roll between them (7), and the disappearance of the clockwise rolls resulting in three much smaller vertically staggered corotating rolls (8). From this point, the branch extends to large values of Ra and was not calculated. Interestingly, unlike in the $\alpha = 0$ case, the size of the convective region in the localized patterns (1) to (8) remains roughly constant and quite small.

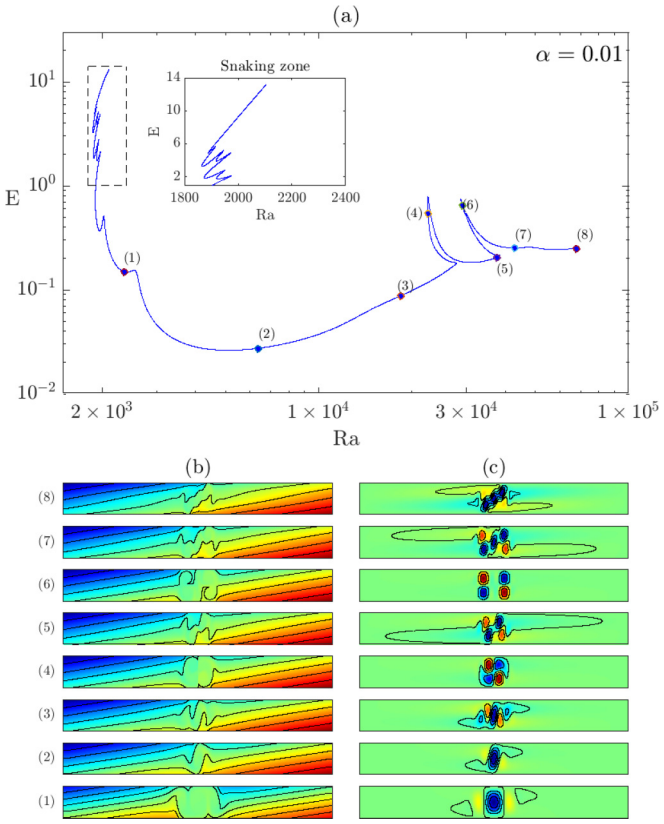

FIG. 4. (a) Solution branch obtained by numerical continuation of the lowest part of the CCW snaking odd branch of convectons (counterclockwise central roll in the snaking region) when the Rayleigh number Ra is increased for $\alpha = 0.01$. The inset shows an enlargement of part of the snaking zone. Contour plots of (b) concentration C and (c) stream function Ψ at the locations indicated in panel (a). In the concentration contours the same color bar is used for all states. Parameters: $S = -0.1$, $\tau = 0.01$, $\sigma = 7$, and $\Gamma = 14$.

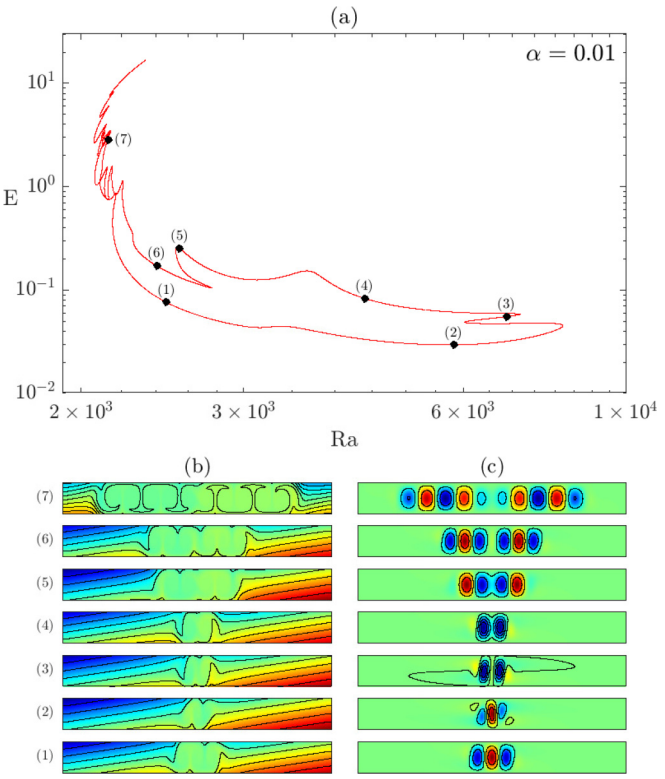

FIG. 5. (a) Solution branch obtained by numerical continuation of the lowest part of the CW odd snaking branch of convectons (clockwise central roll in the snaking region) when the Rayleigh number Ra is increased for $\alpha = 0.01$. Contour plots of (b) concentration C and (c) stream function Ψ at the locations indicated in panel (a). In the concentration contour plots the same color bar is used for all states. Parameters: $S = -0.1$, $\tau = 0.01$, $\sigma = 7$, and $\Gamma = 14$.

Figure 5 shows the results obtained when the lowest part of the CW odd branch of convectons (clockwise central roll in the snaking region) is continued to large values of Ra (up to Ra $\approx 10^4$) for an inclination of $\alpha = 0.01$. Figure 5(a) shows the kinetic energy as a function of Ra, and Figs. 5(b) and 5(c) the contour plots of concentration C and stream function Ψ at the locations indicated in Fig. 5(a). The CW branch suddenly turns around at Ra $\sim$ 8200 and reenters the snaking region. The contour plots corresponding to solution (2) show that, right before the turning point, the convective region of the localized pattern is quite small and consists of a single-pulse state with a central clockwise roll surrounded by a counterclockwise roll on each side. The curve of solutions undergoes a subsequent back and forth between Ra $\sim$ 6020 and Ra $\sim$ 7180, where the central clockwise roll is swept away and the lateral counterclockwise rolls are reinforced (3). As Ra decreases, these two corotating rolls merge (4) and add a clockwise roll on each side (5). In an additional back and forth oscillation of the curve between Ra $\sim$ 2420 and Ra $\sim$ 2720, the single pulse starts to split and turns into a two-pulse state. Then the state undergoes two-pulse snaking within the same snaking region as the single-pulse states, much as occurs in the $\alpha = 0$ case when the lateral boundary conditions are nonperiodic [9].

3. *Tilted* $\alpha = 0.03$ *cell: Two-pulse snaking and corotating localized patterns*

For $\alpha = 0.03$, the outcome of the numerical continuation in Ra of the lowest part of the two odd snaking branches, with clockwise and counterclockwise central rolls, respectively, is completely different from that of the $\alpha = 0.01$ case. As we will see below, the behavior of the lowest part of the snaking branches is, in fact, extremely sensitive to the precise value of the small inclination α and to the type of branch which is analyzed (clockwise or counterclockwise central rolls).

Figure 6 shows the results obtained when the lowest part of the CCW branch of odd convectons (counterclockwise central roll in the snaking region) is continued to large values of Ra (up to Ra $\approx 10^4$) for an inclination of $\alpha = 0.03$. Figure 6(a) shows the kinetic energy as a function of Ra, and Figs. 6(b) and 6(c) the contour plots of concentration C and stream function Ψ at the locations indicated in Fig. 6(a). We can appreciate in the contour plots that the CCW branch undergoes a transition to the two-pulse states, as happened in the CW branch for an inclination of $\alpha = 0.01$. The solution in the lowest part of the snaking branch consists of a single pulse state, with a counterclockwise roll located in the center of

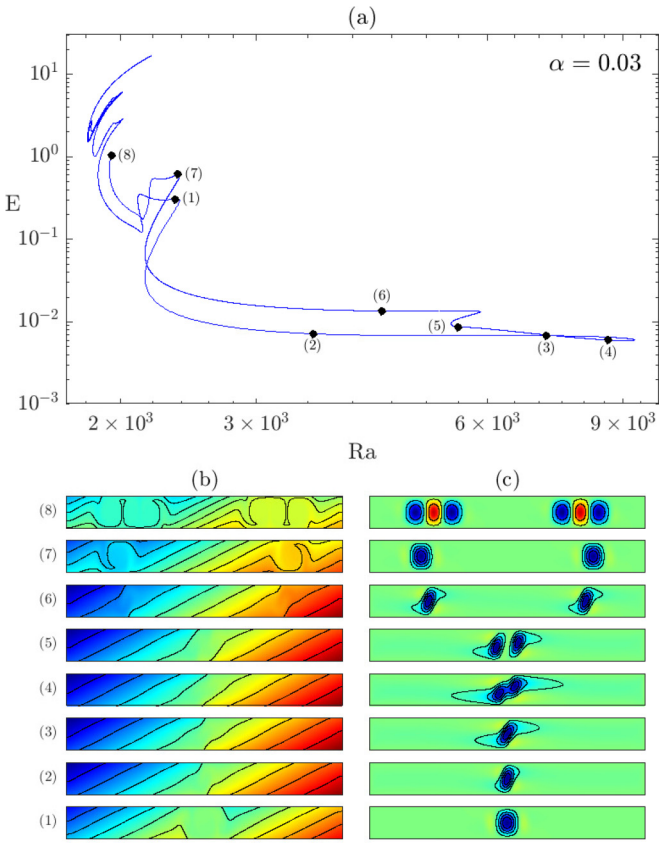

FIG. 6. (a) Solution branch obtained by numerical continuation of the lowest part of the CCW odd snaking branch of convectons (counteclockwise central roll in the snaking region) when the Rayleigh number Ra is increased for $\alpha = 0.03$. Contour plots of (b) concentration C and (c) stream function Ψ at the locations indicated in panel (a). In the concentration contour plots the same color bar is used for all states. Parameters: $S = -0.1$, $\tau = 0.01$, $\sigma = 7$, and $\Gamma = 14$.

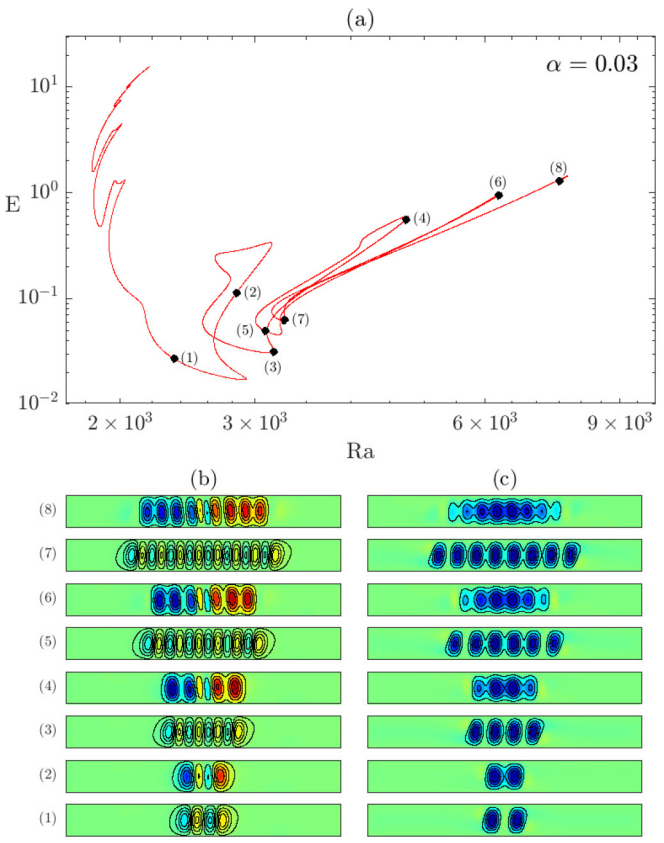

FIG. 7. (a) Solution branch obtained by numerical continuation of the lowest part of the CW odd snaking branch of convectons (clockwise central roll in the snaking region) when the Rayleigh number Ra is increased, for $\alpha = 0.03$. Contour plots of (b) deviation of temperature Θ and (c) stream function Ψ at the locations indicated in panel (a). In the temperature contour plots the same color bar is used for all states. Parameters: $S = -0.1$, $\tau = 0.01$, $\sigma = 7$, and $\Gamma = 14$.

the domain (1). Following the branch as Ra increases, the roll tilts and expands slightly [patterns (2) and (3)]. After a fold at Ra = 9315, the roll nucleates (4) and splits into two counterclockwise rolls (5) before the branch undergoes a back and forth between Ra $\sim$ 5380 and Ra $\sim$ 5876. From this zone, the two rolls move away towards the lateral boundaries (6). When Ra decreases, the tilt of the lateral rolls disappears (7), each of them adds a pair of rolls, so that the localized patterns become two-pulse states (8) that undergo two-pulse snaking within the same snaking region as the single pulse states. Notice that the two-pulse states for $\alpha = 0.03$ [(8) in Fig. 6] and for $\alpha = 0.01$ [(6) in Fig. 5], share the same spatial structure even though they originate from different branches (CCW and CW, respectively).

Figure 7 shows the results obtained when the lowest part of the CW odd branch of convectons (clockwise central roll in the snaking region) is continued to large values of Ra (up to Ra $\approx 10^4$) for an inclination of $\alpha = 0.03$. Figure 7(a) shows the kinetic energy as a function of Ra, and Figs. 7(b) and 7(c) the contour plots of temperature Θ and stream function Ψ at the locations indicated in Fig. 7(a). We choose to represent temperature rather than concentration contours to visualize better the features of the solutions in this branch. The behavior of the branch is completely different from that of the previous branches discussed. The outcome of the numerical continuation reveals a branch with subsequent forward regions of increasing energy followed abruptly by backwards regions in which the energy decreases.

Notice that the localized patterns at the early stages of the continuation consist of two counterclockwise rolls located at the center of the domain, the central clockwise roll has been swept away since the beginning, as can be appreciated in (1), the first solution represented in Fig. 7. The solutions near the folds with lowest values of kinetic energy [solutions around (1), (3), (5), and (7)] consist of localized counterclockwise corotating rolls with an increasing even number of rolls, 2, 4, 6, and 8, respectively, and a concentration gradients inside them (not shown here). A counterclockwise roll is added on both sides in each excursion in which the kinetic energy increases and decreases abruptly. Thus, the size of the convective region in these localized solutions increases progressively. This type of localized solutions composed of counterclockwise corotating rolls was already observed in doubly diffusive convection in vertical slots [28,29], but in the present case this occurs for a very small inclination.

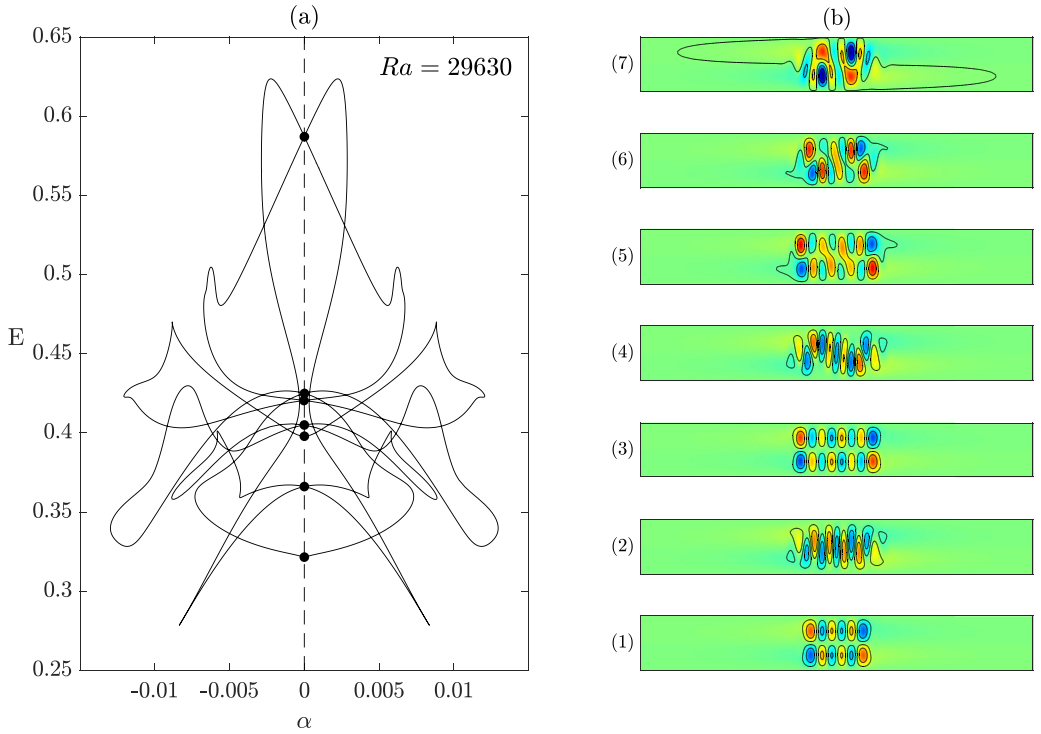

FIG. 8. (a) Complex solution branch obtained by numerical continuation in α of the steady small amplitude odd localized state at Ra = 29 630 in Fig. 3. (b) Contour plots of the stream function Ψ at the locations indicated in panel (a) and where the number of each solution increases from bottom to top. Parameters: $S = -0.1$, $\tau = 0.01$, $\sigma = 7$, and $\Gamma = 14$.

On the other hand, the solutions near the folds with higher values of kinetic energy [solutions around (2), (4), (6), and (8)] correspond to an interesting new type of localized solution we never observed before. Essentially, these patterns consist of a sequence of tightly packed counterclockwise rolls, located in the central part of the cell, with a smaller wavelength than that of the previous corotating-roll patterns from which they derive. Their most remarkable feature is the temperature field. Regardless of whether the fluid is ascending or descending, the left-half part of the convective region corresponds to cold fluid, while the right-half part corresponds to warm fluid, with the exception of a very small central region where cold descending fluid and warm ascending fluid is observed. A counterclockwise central circulation associated to the inclination, i.e., a natural flow with ascendent warmer fluid and descendent colder fluid, appears to be superposed to the distribution of localized rolls. These type of solutions are therefore expected to exist only in inclined containers, as computations will confirm. The concentration field (not showed here) is almost uniform within the sequence of rolls. We followed this curve until a fold value of ∼7690. From this point the branch has not been calculated.

B. Numerical continuation of small-amplitude localized solutions with respect to α

In this section we want to investigate whether some of the striking small amplitude localized states that we describe in the previous section survive or not when the inclination α of the cell is modified. To do this, we carried out a numerical continuation of a choice of initial localized states, taking as continuation parameter the inclination α of the cell and fixing the value of Ra. Following this strategy, we are able to identify, on one hand, localized states existing in the noninclined $\alpha = 0$ cell that are completely different from those shown in Fig. 3, and on the other, localized states that require inclination of the cell to exist. We describe such localized states hereafter.

The first localized solution that we continued is solution (6) in Fig. 3, one of the small-wavelength localized states obtained in the noninclined cell when the odd convecton snaking branch is continued in its lowest part for large values of the Rayleigh number. The value of Ra now is fixed to Ra = 29 630 and the inclination α is allowed to vary. The outcome of the numerical continuation is summarized in Fig. 8, where we represent the energy E of the different visited states as a function of the value of α. Notice that, as a consequence of the $R_{1,\alpha}$ symmetry, the resulting plot is symmetric with respect to $\alpha = 0$. Figure 8(a) shows the solution branch and Fig. 8(b) shows the countour plot of the stream function, numbered from bottom to top, at the points indicated in Fig. 8(a), which correspond to all the crossing points of the curve with the $\alpha = 0$ axis.

We observe that (i) the solution branch is closed, (ii) it extends up to $\alpha = 0.013$, and (iii) for some of the solutions obtained for $\alpha = 0$ [i.e., solutions (1) and (3)] the curve crosses the $\alpha = 0$ axis only once, while for other [i.e. solutions (2), (4), (5), (6), and (7)], the curve crosses the $\alpha = 0$ axis twice. This last feature of the curve can be understood in terms of the symmetries of the $\alpha = 0$ system. Each of the points in the $\alpha = 0$ axis correspond to two solutions: the solution plotted in Fig. 8(b), and their transformation by the

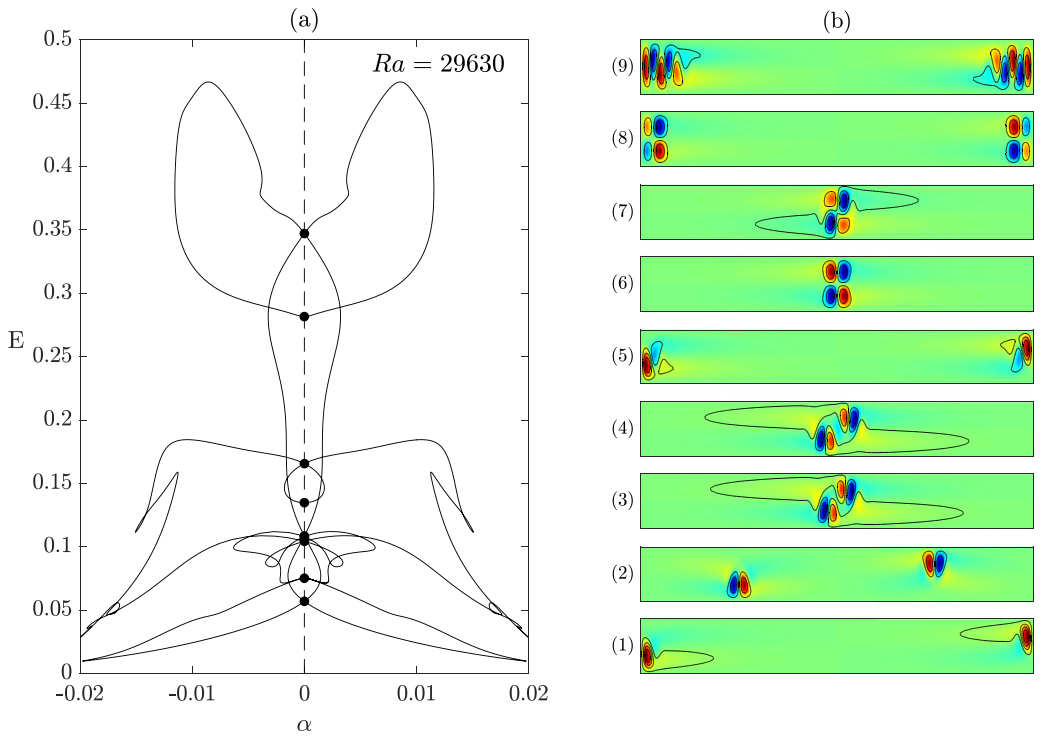

FIG. 9. (a) Complex solution branch obtained by numerical continuation in α of the steady small amplitude odd localized state at Ra = 29 630 [state (4) in Fig. 4]. (b) Contour plots of the stream function Ψ at the locations indicated in panel (a) and where the number of each solution increases from bottom to top. Parameters: $S = -0.1$, $\tau = 0.01$, $\sigma = 7$, and $\Gamma = 14$.

R_1 symmetry. Compare, for example, solutions (6) in Fig. 3 and (2) in Fig. 8, they are related by the R_1 symmetry. When α varies each representation of the same solution follows a different path since, for $\alpha \neq 0$, the R_1 transformation is no longer a symmetry of the problem. Thus, while at points (2), (4), (5), (6), and (7) the curve crosses the $\alpha = 0$ axis twice, solutions (1) and (3), apart from being R invariant, are also R_1 invariant and the curve crosses these points only once.

Performing a continuation with respect to α allows to obtain alternative localized structures for a fixed value of the Rayleigh number. Apart from the initial small-wavelength localized state [solution (6) in Fig. 3, which corresponds to (2) in Fig. 8], we obtain localized solutions in the form of (i) several stacked pairs of rolls [three pairs of rolls in (1), four pairs in (3)], (ii) misaligned pairs of rolls [solution (4)], (iii) coexisting stacked and nonstacked pairs of rolls [solutions (5) and (6)], and (iv) stacked clockwise and counterclockwise rotating rolls [solution (7)]. Despite the different spatial structure of these patterns, the size of the convective region remains approximately constant in these localized structures.

The second localized solution that we continued is located in the extension of the lowest part of the snaking CCW curve for $\alpha = 0.01$, near solution (4) in Fig. 4, and consists of two pairs of vertical stacked rolls. Again, the value of Ra is fixed to Ra = 29 630 and the inclination α is allowed to vary. The result of the numerical continuation is summarized in Fig. 9. Figure 9(a) shows the solution branch and Fig. 9(b) shows the countour plots of the stream function, numbered from bottom to top, at the points indicated in Fig. 9(a), which correspond to the crossing of the curve with the $\alpha = 0$ axis.

Starting from the mentioned solution for $\alpha = 0.01$ [solution near (4) in Fig. 4], and following the branch by decreasing α, the first crossing with the $\alpha = 0$ axis is solution (7) of Fig. 9. Further advancing the continuation branch, we obtain a closed symmetric curve that extends to $\alpha = 0.02$, with double crossing points [solutions (1) to (5) and (7)] and single crossing points for R_1-invariant solutions [solutions (6) and (8)]. This resulting closed curve is different from the previous one and corresponds to localized solutions of completely different spatial features.

Among the variety of localized solutions found throughout the curve, we focus on those visited by the curve in the crossing with the $\alpha = 0$ axis, that is, we describe the localized solutions arising in the horizontal cell. We can distinguish clearly that, while in some of the localized solutions the convective region is located in the center of the cell, in others, the conductive regime fills the central part of the cell and the convective motions take place near the lateral boundaries. Solutions (6) and (7) consist of two stacked pairs of rolls in the center of the domain. Whereas (6) is R_1 invariant, the weakening of the rotating clockwise rolls in (7) breaks the R_1 invariance. Solution (3) is formed by two vertical staggered pairs of rolls, which separate slightly away in (4), and move notably towards the lateral walls in (2). Remarkably, in (2), one of the two pairs of rolls remains attached to the bottom part of the cell and the other to the top part. In solution (1), the counterclockwise rotating rolls of every pair are swept away and the remaining clockwise rotating rolls are attached to the lateral walls. We observe that weak counterclockwise rotating rolls reappear again besides the clockwise rotating rolls in solution (5). Finally, the convective region in solutions

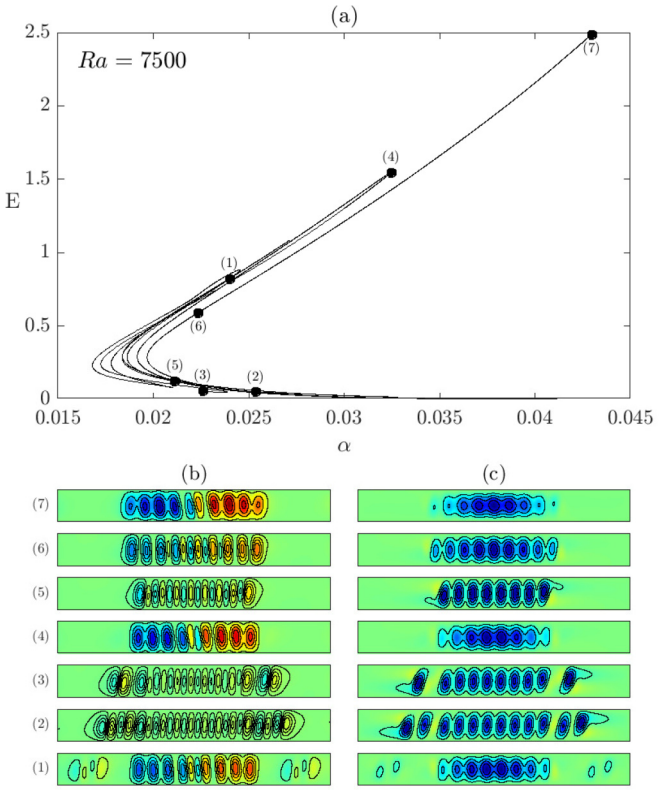

FIG. 10. (a) Complex solution branch obtained by numerical continuation in α of the steady small amplitude odd localized state at Ra $= 7500$ [state (8) in Fig. 7]. Contour plots of (b) the deviation of temperature field Θ and (c) stream function Ψ at the locations indicated in panel (a). In the temperature contours the same color bar is used for all states. Parameters: $S = -0.1$, $\tau = 0.01$, $\sigma = 7$, and $\Gamma = 14$.

(8) and (9) continues to be attached to the lateral walls, but while (9) is formed by two pairs of rolls at each side filling the entire vertical space, convection in (8) is in the form of two stacked pairs of rolls at each side, giving rise to an R_1-invariant solution. As can be appreciated, the size of the convective region of the localized solutions in Fig. 9 is smaller than that of the solutions previously described in Fig. 8.

The third and last localized solution that we continued is obtained in the extension of the lowest part of the CW odd snaking branch of convectons for $\alpha = 0.03$, near solution (8) in Fig. 7, and consists of counterclockwise tightened rolls. As we discussed before, the clockwise rolls were swept in this localized solution. This is a common feature of the solutions when the inclination becomes relevant [17]. Now, the value of Ra is fixed to Ra $= 7500$ and the inclination α is allowed to vary. The outcome of the numerical continuation is summarized in Fig. 10. Figure 10(a) shows the solution branch in a E-α diagram and Figs. 10(b) and 10(c) show, for the points indicated in Fig. 10(a), the countour plots of the deviation of temperature field Θ and the stream function Ψ, respectively.

In this case, the numerical continuation unveils a branch with back and forth regions of increasing and decreasing kinetic energy organized around a vertex located at $\alpha \sim 0.019$. The initial state for the numerical continuation is a solution near (4) in Fig. 10. From this state, the numerical continuation leads to subsequent increases and decreases of α. The behavior of the solutions visited resembles that of solutions in Fig. 7. Solutions (2), (3), and (5) have a low value of the kinetic energy, and are standard localized counterclockwise corrotating rolls with a varying number of rolls and a concentration gradient inside them. Solutions (4) and (7) have higher values of the kinetic energy and are composed of counterclockwise tightened rolls, with colder fluid inside the left-half rolls and warmer fluid inside the right-half rolls, regardless of whether the fluid is ascending or descending. The concentration field, not shown here, is almost uniform inside the sequence of rolls. Finally, solutions (1) and (6) have intermediate values of E and appear to be transition patterns with mixed features of the two types of patterns described previously.

This branch of solutions does not cross the $\alpha = 0$ axis, in agreement with the fact that inclination is responsible for the existence of these peculiar patterns. In addition, the curve does not appear to close itself, so the curve could be extended from (7) and from a point near (1).

IV. SUMMARY AND CONCLUDING REMARKS

Binary mixture convection in two-dimensional elongated and horizontal closed rectangular cells heated from below can be in the form of steady roll-like localized structures called *convectons*. These structures organize in the parameter space (kinetic energy-Rayleigh number) in a pair of intertwined snaking branches with different symmetries (even and odd convectons). In this paper, we continued the lowest part of the branch of odd convectons up to large values of the Rayleigh number and it does not connect to the base conductive state. Instead, a marked increase of the kinetic energy is observed, associated to a slow growth of the size of the convective region in the localized structure. Localized states in the form of tightly packed convective rolls that progressively decrease their wavelength are obtained. This behavior is also observed in rectangular cells with periodic boundary conditions in the lateral walls.

Previous studies in related *laterally periodic* systems that also exhibit snaking reported a different behavior of the lowest part of the snaking branches. These systems included natural double diffusive convection in a vertical slot with imposed competing temperature and concentration horizontal gradients perpendicular to the buoyancy force and periodic boundary conditions in the vertical direction, double diffusive convection in a horizontal layer with imposed temperature and concentration differences between the horizontal walls and periodic boundary conditions in the horizontal direction and the subcritical Swift-Hohenberg equation [12,15]. In these configurations the lowest part of the snaking branches emerges from a branch of spatially periodic states in a secondary Eckhauss instability at moderate values of the Rayleigh number. This branch of periodic states bifurcates from the conduction state. In contrast, in binary mixture convection, with periodic boundary conditions and negative-enough Soret coefficient (a critical value dependent on the Lewis number) [30], the branch of periodic states extends to infinity. Thus, for binary mixtures in rectangular containers with periodic lateral walls, the branch of spatially periodic states neither bifurcates from the conduction state

nor gives rise to the lowest part of the snaking branches. The coupling between temperature and concentration through the Soret effect, rather than the specific boundary conditions considered or the symmetries of the problem, seems to be responsible for the differences in the bifurcation diagrams.

When a slight inclination of the cell α is introduced, the numerical continuation with Ra of the lowest part of the two odd snaking branches resulting from the splitting of the odd snaking branch, reveals a behavior different from the horizontal case. The energy of the branches no longer increases monotonically when the Ra number is increased, as it occurs for $\alpha = 0$, and the behavior is very sensitive to the precise value of α and to the type of branch. In some occasions, the branches even turn around in a fold and eventually reenter the snaking region in the form of two-pulse localized solutions. In others, the convective region of the localized pattern remains rather small while the amplitude of the solution slowly grows. Finally, there are also new families of localized solutions, with a larger convective region, and for which the temperature field and the vertical velocity are out of phase. In all the cases, their spatial properties differ considerably from those of convectons.

In the search for the origin of these alternative localized states obtained in slightly inclined cells, we performed a numerical continuation with the inclination of the cell α. Starting from the localized solutions at Ra values far from the snaking zone, we obtain complex diagrams with intricate branches of solutions. We observe qualitatively different behaviours when the continuation is initiated from localized solutions belonging to branches obtained for small values of α, $\alpha = 0$, and $\alpha = 0.01$, or to branches obtained for slightly larger values of α, $\alpha = 0.03$.

The complex branches obtained by continuation of solutions belonging to $\alpha = 0$ and $\alpha = 0.01$ turn out to be closed symmetric with respect to the continuation parameter α, and cross several times the $\alpha = 0$ location. This means that, unexpectedly, a variety of highly localized states coexist for the same heating, not only in the inclined cell, but also in the horizontal case. By simply computing two of these closed branches, we are able to obtain 16 different localized solutions coexisting for the same value of Ra for the $\alpha = 0$ cell. Some of these solutions have a central convective region made up of several stacked pairs of rolls, misaligned pairs of rolls, or a combination, but in other families of localized solutions the convective region is located out of the central part of the cell and can even be attached to the lateral walls. In some cases the solutions are invariant to both R_1 and R transformations. The existence of these localized solutions is limited to a region of small values of α.

In contrast, when the continuation is initiated from localized solutions obtained for larger values of α, $\alpha = 0.03$, the branches of solutions exhibit complex back and forth oscillations in α, with increasing and decreasing energy, but never reach the $\alpha = 0$ value. These branches do not close on themselves and the spatial features that the solution exhibit are intrinsic to inclination.

To sum up, we explored the lowest part of the snaking branches for different inclinations of the cell. The exploration reveals the existence of localized solutions with very different characteristics from those of convectons. When numerical continuation of these solutions with respect to the inclination of the cell is carried out, we obtained localized solutions organized in isolas or in open branches. Following this procedure, we were able to obtain a variety of localized solutions coexisting for the same heating and inclinations, even in the horizontal cell, that would have been extremely difficult to obtain otherwise.

These localized solutions are highly unstable; when time evolution runs at Ra $\approx 29\,630$ are carried out, taking as initial condition either localized solutions or small amplitude random states, the system evolves quickly towards extended states of pairs of rolls. Despite the fact that these extended states do not exhibit spatial localization, the system remains a long time in transient nonuniform wavelength states. In such states, the patterns exhibit regions in which the wavelength of the convective rolls is close to the critical wavelength and regions with much narrower convective rolls. Very long integration times are needed before narrow rolls widen and almost uniform wavelength states fill the cell.

ACKNOWLEDGMENT

This work was supported by the Spanish Ministry of Science and Innovation under Grant No. PID2020-114043GB-I00.

[1] J. Fineberg, E. Moses, and V. Steinberg, Phys. Rev. Lett. **61**, 838 (1988).
[2] V. Steinberg, J. Fineberg, E. Moses, and I. Rehberg, Physica D **37**, 359 (1989).
[3] P. Kolodner, C. M. Surko, and H. Williams, Physica D **37**, 319 (1989).
[4] P. Kolodner, Phys. Rev. E **47**, 1038 (1993).
[5] O. Batiste, I. Mercader, M. Net, and E. Knobloch, Phys. Rev. E **59**, 6730 (1999).
[6] O. Batiste, E. Knobloch, I. Mercader, and M. Net, Phys. Rev. E **65**, 016303 (2001).
[7] I. Mercader, O. Batiste, A. Alonso, and E. Knobloch, Phys. Rev. E **80**, 025201(R) (2009).
[8] I. Mercader, O. Batiste, A. Alonso, and E. Knobloch, Fluid Dyn. Res. **42**, 025505 (2010).
[9] I. Mercader, O. Batiste, A. Alonso, and E. Knobloch, J. Fluid Mech. **667**, 586 (2011).
[10] P. Kolodner, Phys. Rev. E **48**, R665 (1993).
[11] O. Batiste, E. Knobloch, A. Alonso, and I. Mercader, J. Fluid Mech. **560**, 149 (2006).
[12] C. Beaume, A. Bergeon, and E. Knobloch, Phys. Fluids **23**, 094102 (2011).
[13] K. Ghorayeb and A. Mojtabi, Phys. Fluids **9**, 2339 (1997).
[14] A. Bergeon and E. Knobloch, Phys. Fluids **20**, 034102 (2008).
[15] A. Bergeon, J. Burke, E. Knobloch, and I. Mercader, Phys. Rev. E **78**, 046201 (2008).

[16] C. Beaume, A. Bergeon, and E. Knobloch, J. Fluid Mech. **840**, 74 (2018).
[17] I. Mercader, O. Batiste, A. Alonso, and E. Knobloch, Phys. Rev. E **99**, 023113 (2019).
[18] D. Lo Jacono, A. Bergeon, and E. Knobloch, Phys. Rev. Fluids **2**, 093501 (2017).
[19] A. Azimi and T. M. Schneider, J. Fluid Mech. **912**, A47 (2021).
[20] A. Alonso, I. Mercader, and O. Batiste, Phys. Rev. E **97**, 023108 (2018).
[21] A. Alonso, I. Mercader, O. Batiste, and J. M. Vega, SIAM J. Appl. Dyn. Syst. **21**, 2148 (2022).
[22] I. Mercader, O. Batiste, and A. Alonso, Int. J. Numer. Meth. Fluids **52**, 707 (2006).
[23] S. Hugues and A. Randriamampianina, Int. J. Numer. Meth. Fluids **28**, 501 (1998).
[24] S. Zhao and M. J. Yedlin, J. Comput. Phys. **113**, 215 (1994).
[25] C. K. Mamun and L. S. Tuckerman, Phys. Fluids **7**, 80 (1995).
[26] V. Frayssé, L. Giraud, S. Gratton, and J. Langou, Technical Report No. TR/PA/03/3, CERFACS, 2003.
[27] A. Alonso, O. Batiste, A. Meseguer, and I. Mercader, Phys. Rev. E **75**, 026310 (2007).
[28] R. C. Paliwal and C. F. Chen, J. Fluid Mech. **98**, 755 (1980).
[29] C. F. Chen and S. Thangam, J. Fluid Mech. **161**, 161 (1985).
[30] S. Hollinger and M. Lucke, Phys. Rev. E **52**, 642 (1995).